The electronic gas-phase spectrum of B_3 radical revisited

Łukasz Chacaga, Evan B. Jochnowitz,
Zohra Guennoun, Hongbin Ding[1], John P. Maier*

Department of Chemistry, University of Basel, Klingelbergstrasse 80, CH-4056 Basel, Switzerland

ABSTRACT

The gas-phase electronic spectrum of cyclic-B_3 (D_{3h}) radical has been remeasured in a supersonic molecular beam using a mass-selective resonant 2-color 2-photon technique, leading to a revision of previously reported spectroscopic constants. The species was prepared by ablation of a boron nitride rod in the presence of helium. *Ab intio* calculations on the geometries and vertical electronic excitation energies, as well as mass identification, indicate that the detected band, centered at 21848.77(2) cm^{-1}, is the origin of the $2\,^2E' - \tilde{X}\,^2A'_1$ cyclic-$^{11}B_3$ system. A spectral fit yields the rotational constants as $B'' = 1.2246(45)$ and $C'' = 0.62131(72)$ cm^{-1} in the $\tilde{X}\,^2A'_1$ ground state, and $B' = 1.1914(44)$ and $C' = 0.61173(69)$ cm^{-1} in the excited $2\,^2E'$ state.

© 2008 Elsevier B.V. All rights reserved.

1. Introduction

Electronic gas-phase spectra of a variety of metal containing carbon chain species have recently been obtained by combining the mass selective spectroscopic technique of resonant 2-color 2-photon ionization (R2C2PI) with the production capabilities of a laser ablation source, including MgC_4H and MgC_6H [1], AlCCH [2], and AlC_2 [3]. The same approach also led to the observation of the $B\,^2\Pi_g - X\,^2\Sigma_u^+$ electronic spectrum of gas-phase linear BNB ($D_{\infty h}$), which was rotationally [4] and vibrationally [5] assigned. Because of the measurable quantities of boron trimer produced during ablation of boron nitride we have obtained less congested electronic spectra and more accurate spectral assignments than was possible earlier [6]. In the latter, the gas-phase $2\,^2E' - \tilde{X}\,^2A'_1$ transition of B_3 was recorded using pulsed cavity ringdown spectroscopy, however, the spectrum was littered with overlapping lines due to C_2 Swan bands, neon atomic absorptions, and mixed isotopologues of the probed species themselves. Here, these problems are eliminated by utilizing the mass selection afforded from R2C2PI and providing a reassignment of previously measured rotational constants and a new origin band placement. Laser ablation also proved a more efficient means of B_3 radical production than discharging

$B_{10}H_{14}$ gas [6], allowing the collection of a higher signal to noise spectrum.

Among the three atom trimers studied, few have received as much attention as H_3, first recognized by Herzberg in 1979 through emission in a discharge of hydrogen gas [7–10]. Fluorescence [11] and laser spectroscopic [12] studies have continued, as well as investigations into higher Rydberg states [13–15]. The latter have also been studied in predissociation, given the fact that these lie in the dissociation continuum of the electronic ground state [16]. Other trimers have been investigated using R2C2PI, including Li_3 [17], Na_3 [18], Al_3 [19], Cu_3 [20] and Ag_3 [21]. In general, these trimers tend to distort in geometry from their equilateral triangle D_{3h} structures when found in a degenerate state, thereby splitting their energy levels and complicating the rotational and vibrational analysis.

Boron trimer was investigated initially in rare gas matrices using infrared spectroscopy [22] and electron spin resonance [23], the latter demonstrating that B_3 contains an unpaired electron and three equivalent nuclei in the ground state. Of the low lying states predicted for cyclic-B_3 (D_{3h}), only the $^2A''_2$ and $^2E'$ ones are dipole accessible from the $\tilde{X}\,^2A'_1$ state. Previously the $1\,^2A''_2 - \tilde{X}\,^2A'_1$ electronic transition in B_3 was recorded in 6 K neon matrices through direct absorption, with a clear progression in ν_1 (a'_1) observed in the $^1A''_2$ state [24]. The matrix isolated electronic absorption spectra for the $1\,^2E' - \tilde{X}\,^2A'_1$ and $2\,^2E' - \tilde{X}\,^2A'_1$ transitions of B_3 were also reported with vibrational progressions in the excited state assigned [25]. Later, the origin band of the $2\,^2E' - \tilde{X}\,^2A'_1$ transition was partially rotationally analyzed in the gas-phase using a cavity ring

---

* Corresponding author. Tel.: +41 61 267 38 26; fax: +41 61 267 38 55.
  E-mail address: j.p.maier@unibas.ch (J.P. Maier).
  [1] Present address: School of Physics and Optoelectronic Technology, Dalian University of Technology, Ling-Gong Road No. 2, 116024 Dalian, PR China.
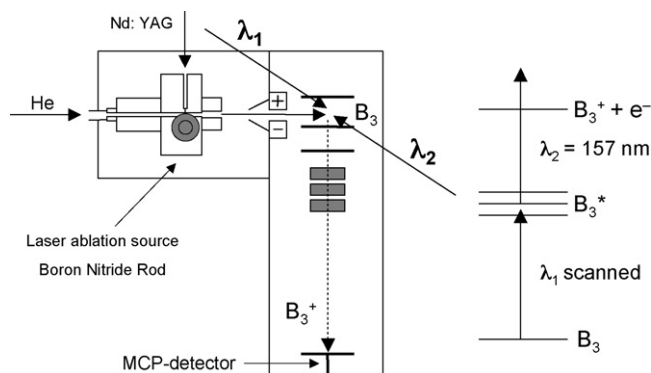
Fig. 1. Experimental setup of the R2C2PI apparatus combined with a laser vaporization source and the 2-color excitation/ionization scheme.

down absorption technique coupled with an electrical discharge of $B_{10}H_{14}$ precursor [6].

2. Experimental

The experimental set-up consists of a molecular beam combined with a linear time of flight (TOF), as shown in Fig. 1 [4]. The laser ablation of a boron nitride rod in the presence of a pulsed He buffer gas (∼5 bar backing pressure) produced B_3 by focusing the 532 nm output of a Nd:YAG laser (30 mJ pulse^{-1}, 5 ns width) onto a rotating and translating rod. The plasma traveled through a 15-mm long and 3-mm diameter channel before expanding into vacuum where the resulting supersonic jet of neutrals and ions passed through a skimmer. A perpendicular electrical field removed ions before they entered the extraction zone of the TOF. There the neutral molecules were ionized by an F_2 excimer laser (157 nm) and the resulting cations were extracted using a pulsed electrical field. The ionization process, as shown in the right of Fig. 1, is more efficient when the tunable laser is resonant with a dipole-allowed electronic transition. After traveling through a 1.2-m flight tube a multichannel plate ion detector collected the signal which was fed to an oscilloscope followed by data acquisition. R2C2PI spectra of B_3 were measured by monitoring the mass-peak area as a function of laser wavelength, with UV excitation photons provided from a pulsed excimer pumped dye laser (0.15 cm^{-1} bandwidth, ∼0.5–1 mJ pulse^{-1}). Because the R2C2PI spectra are mass selective, $^{11}B_3$ ($m/z = 33$) could be measured without overlapping isotopologues or other species. A wavemeter provided the calibration.

Table 2
Calculated energies (a.u.), bondlengths (Å) and rotational constants (cm^{-1}) for the $\tilde{X}\,^2A_1'$ ground state of cyclic-B_3 (D_{3h}) at the RCCSD(T) approach using assorted basis sets

Method	Basis set	Energy	Bond length	A	B	C
RCCSD(T)	cc-pVDZ	−74.04547	1.6086	1.2054	1.2054	0.6027
	cc-pVTZ	−74.09701	1.5727	1.2611	1.2611	0.6305
	cc-pVQZ	−74.11336	1.5642	1.2748	1.2748	0.6374
	aug-cc-pVTZ	−74.09998	1.5718	1.2625	1.2625	0.6312
	aug-cc-pVQZ	−74.11449	1.5643	1.2746	1.2746	0.6373
MRCI[a]			1.5707	1.2643	1.2643	0.6321

[a] Ref. [25].

3. Results and discussion

3.1. Theoretical results

3.1.1. Ground state

Previous theoretical studies on the B_3 radical calculated the ground state structure using UHF and MCSCF levels of theory combined with smaller basis sets [26,27]. Here the equilibrium geometries have been optimized at the B3LYP level [28] and the RCCSD(T) approach with an aug-cc-pVQZ basis set [29]. The resulting bond lengths, harmonic vibrational frequencies and rotational constants B_e are collected in Table 1. The cyclic-B_3 (D_{3h}) isomer is the most stable structure (global minimum), with an $\tilde{X}\,^2A_1'$ ground state. Bent B_3 (C_{2v}), linear B_3 ($D_{\infty h}$) and linear B_3 ($C_{\infty v}$) are local minima found ∼1.7 eV above the cyclic D_{3h} structure.

For the B_3 (D_{3h}) isomer higher level calculations were later carried out using the RCCSD(T) approach with systematic sequences of Dunning's correlation-consistent basis set. The calculated rotational constants are given in Table 2, along with previously reported multi-reference configuration interaction (MRCI) electronic structure calculations [25].

3.1.2. Excited state

Previously MRCI *ab initio* electronic structure calculations were performed with extended reference space to help interpret the complex vibronic structure observed in the Jahn-Teller active excited $^2E'$ states of B_3 [25]. The T_0 values for the three allowed transitions were found as: $1\,^1A_2' - \tilde{X}\,^2A_1'$ at 0.78 eV, $1\,^2E' - \tilde{X}\,^2A_1'$ at 1.59 eV and $2\,^2E' - \tilde{X}\,^2A_1'$ at 2.76 eV.

In this study investigations of the excited electronic states for B_3 (D_{3h}) were carried out using the complete active space self-consistent field (CASSCF) and MRCI theory [30]. A list of vertical electronic transition energies are compared in Table 3, computed using the GAUSSIAN 98 [31] and MOLPRO programs [32]. It is of note in Table 3 that as only transitions to $^2A_2''$ and $^2E'$ states are dipole allowed, these carry the oscillator strength. The ordering for the

Table 1
Calculated geometry (Å), rotational constant B_e and harmonic frequencies ω (cm^{-1}) for the ground state B_3 isomers at the B3LYP level of theory using an aug-cc-pVQZ basis set

Isomer	State	Geometry	B_e	ω_1	ω_2	ω_3
B_3 ($D_{\infty h}$)	$X\,^2\Pi_u$	$r = 1.5415$	$B = 0.3338$	$902(\sigma_g)$	$129(\pi)/63(\pi)$[a]	$1509(\sigma_u)$
B_3 (D_{3h})	$\tilde{X}\,^2A_1'$	$r = 1.5406$	$A = B = 1.2904$ $C = 0.6452$	$1229(a_1')$	$944(e')$	$944(e')$
B_3 (C_{2v})	$\tilde{X}\,^4A_2$	$r_1 = 1.5698$ $r_2 = 1.5698$ $r_3 = 1.8871$	$A = 1.4594$ $B = 0.86004$ $C = 0.5411$	$1077(a_1)$	$421(a_1)$	$1011(b_2)$
B_3 ($C_{\infty v}$)	$X\,^2\Sigma^+$	$r_1 = 1.5313$ $r_2 = 1.5217$	$B = 0.3286$	$1468(\sigma)$	$181(\pi)/191(\pi)$[a]	$860(\sigma)$

[a] A difficulty arises when calculating the bending vibration of the linear triatomics. The bending motion splits the degenerate potential into two nondegenerate A' and A'' potentials with two distinct frequencies.

Table 3
Calculated vertical transition energies T_v (eV) and oscillator strengths, f, using CASSCF, MRCI and MRCI+Q theories with cc-pVTZ basis set for cyclic-B_3.

Isomer	Transition	T_v			f	
		CASSCF	MRCI	MRCI+Q	CASSCF[a]	CASSCF
B_3 (D_{3h})	$1\,^2A_2'' - \tilde{X}\,^2A_1'$	0.868	0.824	0.827	0.878	3.6×10^{-3}
	$1\,^2E' - \tilde{X}\,^2A_1'$	1.701	1.749	1.691	1.870	6.0×10^{-3}
	$2\,^2E' - \tilde{X}\,^2A_1'$	2.997	2.825	2.638	3.385	1.5×10^{-3}
	$1\,^2E'' - \tilde{X}\,^2A_1'$	3.120	2.883	2.812	2.296	0.0
	$2\,^2E'' - \tilde{X}\,^2A_1'$	4.517	4.147	3.908	4.824	0.0

[a] Ref. [27].

occupied orbitals of B_3 (D_{3h}) is: $1a_1'$, $1e'$, $2a_1'$, $2e'$, $1a_2''$, $3a_1'$, resulting in a $^2A_1'$ ground state, as confirmed through electron spin resonance investigations [23]. The lower unoccupied orbitals, from DFT calculations, are: $3e'$, $1e''$, $4e'$, $1a_2'$. Transitions to the $^2E'$ states thus arise from two different low-lying excitations: $3e' \leftarrow 3a_1'$ and $3a_1' \leftarrow 2e'$. Both of these, $1\,^2E' - \tilde{X}\,^2A_1'$ and $2\,^2E' - \tilde{X}\,^2A_1'$, have been observed through absorption in Ne matrices at 13,587 and 21,828 cm^{-1}, respectively [25]. The transition observed in this study, located near 21,849 cm^{-1} is the origin band of the $2\,^2E' - \tilde{X}\,^2A_1'$ system.

3.2. Rotational structure

The rotational structure for the origin band of the $2\,^2E' - \tilde{X}\,^2A_1'$ transition of $^{11}B_3$ is shown in Fig. 2. This pattern was observed earlier by measurement of the absorption spectrum using cavity ring down spectroscopy (CRDS) [10], however, there was no mass-selection and therefore lines of the naturally occurring boron isotopologues overlapped. Here the structure is selectively recorded for $^{11}B_3$ (Fig. 2), exhibiting rotationally resolved P and R branches (0.15 cm^{-1} resolution). An analysis was carried out with a conventional hamiltonian for a symmetric top D_{3h} molecule using the spectral simulation program PGOPHER [33]. Where possible distinct lines were fit for a $^2E' - \tilde{X}\,^2A_1'$ transition. The intensities of the peaks are rather qualitative because of fluctuations in the radical source's output.

The rotational analysis assumes D_{3h} symmetry. The radical possesses three identical atoms of nuclear spin 3/2 thus leading to an alternation of statistical weights as a function of K, with populations originating from $K \neq 3n$ lower than those from $K = 3n$ [34]. In addition, because of the D_{3h} symmetry, there is further alternation in J with those from $K = 0$. Overall, the intensity distribution
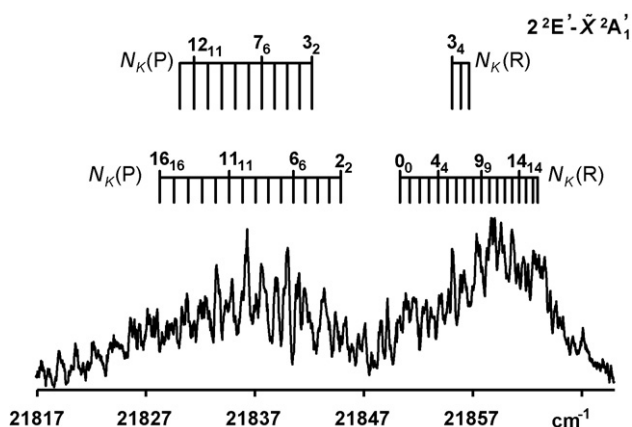

Fig. 2. The $2\,^2E' - \tilde{X}\,^2A_1'$ electronic transition of $^{11}B_3$ (D_{3h}) measured using a resonant 2-color 2-photon ionization technique in a supersonic molecular beam.

Table 4
Statistical weights of the rovibronic states of $^{11}B_3$ (D_{3h})

Nuclear spin symmetry	Statistical weight	Rovibronic symmetry
A_1	20	A_2', A_2''
A_2	4	A_1', A_1''
E	20	E', E''

in the rotational fine structure for the perpendicular band will be determined by the Hönl-London factors, a Boltzmann distribution, and the statistical weights g_{KJ}. Briefly, because of three identical ^{11}B atoms ($I = 3/2$), the total wavefunction of $^{11}B_3$ must be antisymmetric under permutation of two nuclei. In the D_3 subgroup an A_1 wavefunction is symmetric, while A_2 is antisymmetric under two-fold exchange of nuclei. Therefore, the total wavefunction of $^{11}B_3$, when combining the rovibronic and nuclear spin functions, must have an overall symmetry of A_2. With this in mind, the statistical weights, obtained from the number of suitable nuclear spin states which give the total wavefunction A_2 symmetry [35], are given in Table 4.

Although the B_3 radical in a $^2E'$ state will undergo a deformation, according to the Jahn-Teller effect, we have neglected such a geometry change in this analysis. Ignoring this breaking of an equilateral triangle structure in the excited state is justified due to the excited state's low stabilization energy as compared to its zero point energy in the $2\,^2E'$ state (39 cm^{-1} versus 1522 cm^{-1}, as calculated) [25], therefore, offering little gain in energy through distorting from its D_{3h} symmetry. The only slight deformation experienced in the $2\,^2E'$ state of B_3 results in an altered bond angle of 60.9° (from calculation [25]). In contrast, Li_3 in its excited $A\,^2E''$ state opens to an experimentally determined bond angle of 76.4° [17]. Thus, D_{3h} symmetry is assumed for the excited state in the rotational analysis of B_3, giving a quasi "D_{3h}–D_{3h}" transition and allowing for a more straightforward simulation. Of note is the fact

Table 5
Observed rotational lines (in cm^{-1}) of the origin band of the $2\,^2E' - \tilde{X}\,^2A_1'$ system of cyclic-$^{11}B_3$ (D_{3h})

P branch			R branch		
N_K	$\tilde{\nu}_{obs}$	$\tilde{\nu}_{obs} - \tilde{\nu}_{calc}$	N_K	$\tilde{\nu}_{obs}$	$\tilde{\nu}_{obs} - \tilde{\nu}_{calc}$
$1_1 - 2_2$	21844.87	−0.01	$1_1 - 0_0$	21850.31	0.01
$2_2 - 3_3$	21843.82	−0.01	$2_2 - 1_1$	21851.22	−0.01
$3_3 - 4_4$	21842.74	0.04	$3_3 - 2_2$	21852.11	−0.01
$2_1 - 3_2$	21842.23	−0.01	$4_4 - 3_3$	21852.99	−0.01
$4_4 - 5_5$	21841.64	−0.02	$5_5 - 4_4$	21853.84	−0.01
$3_2 - 4_3$	21841.11	−0.01	$6_6 - 5_5$	21854.67	−0.02
$5_5 - 6_6$	21840.52	−0.02	$5_4 - 4_3$	21855.11	−0.01
$4_3 - 5_4$	21839.97	−0.02	$7_7 - 6_6$	21855.48	−0.02
$6_6 - 7_7$	21839.39	−0.03	$6_5 - 5_4$	21855.89	−0.02
$5_4 - 6_5$	21838.80	−0.02	$8_8 - 7_7$	21856.27	−0.03
$7_7 - 8_8$	21838.23	−0.03	$7_6 - 6_5$	21856.66	−0.02
$6_5 - 7_6$	21837.62	−0.03	$9_9 - 8_8$	21857.05	−0.03
$8_8 - 9_9$	21837.05	−0.04	$10_{10} - 9_9$	21857.80	−0.04
$7_6 - 8_7$	21836.42	−0.04	$11_{11} - 10_{10}$	21858.53	−0.05
$9_9 - 10_{10}$	21835.86	−0.05	$12_{12} - 11_{11}$	21859.24	−0.06
$8_7 - 9_8$	21835.20	−0.05	$13_{13} - 12_{12}$	21859.93	−0.07
$10_{10} - 11_{11}$	21834.64	−0.06	$14_{14} - 13_{13}$	21860.61	−0.08
$9_8 - 10_9$	21833.95	−0.05	$15_{15} - 14_{14}$	21861.26	−0.09
$11_{11} - 12_{12}$	21833.40	−0.07	$16_{16} - 15_{15}$	21861.89	−0.10
$10_9 - 11_{10}$	21832.69	−0.06	$17_{17} - 16_{16}$	21862.50	−0.12
$12_{12} - 13_{13}$	21832.14	−0.08			
$11_{10} - 12_{11}$	21831.41	−0.07			
$13_{13} - 14_{14}$	21830.87	−0.09			
$12_{11} - 13_{12}$	21830.11	−0.09			
$14_{14} - 15_{15}$	21829.01	−0.10			
$15_{15} - 16_{16}$	21828.25	−0.12			

The uncertainty of the $\tilde{\nu}_{obs}$ values is judged to be ±0.02 cm^{-1}.

Table 6
Spectroscopic constants determined from the analysis of the $2\,^2E' - \tilde{X}\,^2A_2''$ electronic band system of $^{11}B_3$ (D_{3h})

Parameter	This study		CRDS[a]		Theory[b]	
	$\tilde{X}\,^2A_1'$	$2\,^2E'$	$\tilde{X}\,^2A_1'$	$2\,^2E'$	$\tilde{X}\,^2A_1'$	$2\,^2E'$
T_0 (cm^{-1})		21848.77(2)		21853.52		22723
B (cm^{-1})	1.2246(45)	1.1914(44)	1.19064(157)	1.16825(138)	1.2643	
C (cm^{-1})	0.62131(72)	0.61173(69)	0.59532(79)	0.58412(69)	0.6321	

Values in parentheses denote the 2σ standard deviation from the fit.
[a] Ref. [6].
[b] Ref. [25].

that calculations indicate a stronger Jahn-Teller influence in other excited states of B_3, including the $1\,^2E'$ state, thus prohibiting the use of such assumptions in these transitions [25]. This is evident when examining the matrix absorption spectra [25]; complex vibronic structure observed in the $1\,^2E' - \tilde{X}\,^2A_1'$ transition indicates an excitation to a more distorted excited state than the more simple, more regular progression observed in the $2\,^2E' - \tilde{X}\,^2A_1'$ system. In addition, a dominant origin band in the latter signifies little geometry change on passing from its ground to excited state, further justifying an assumed "D_{3h}–D_{3h}" transition in this instance.

The rovibronic selection rules for a symmetric top "D_{3h}–D_{3h}" transition are: $A_1' \leftrightarrow A_2'', A_2' \leftrightarrow A_2''$, and $E' \leftrightarrow E''$. For the overall $E' - A_1'$ system one expects a transition perpendicular to the top axis, resulting in $\Delta K = \pm 1$, $\Delta J = 0, \pm 1$. Rotational line assignments were made by comparing the observed spectral lines with those from simulation. Immediately two progressions were observed when fitting the spectrum, as shown in Fig. 2: $J'_{K'=J'} - J''_{K''=J''}$ and $J'_{K'=J'-1} - J''_{K''=J''-1}$, where lines with $J = K$ corresponding to the maximum K for a given form the most prominent series. These transitions can be strongly affected by Coriolis coupling, and therefore in the degenerate E'' state one expects a non-zero Coriolis coupling constant, ζ. However, ζ was heavily correlated with the C rotational constants, making its determination uncertain. Nevertheless, a non-zero ζ was crucial in obtaining a reasonable fit of the five varied spectroscopic parameters (T_0, B'', B', A'', and A'). Thus, a final value of $\zeta = \sim 0.2$ cm^{-1} was estimated while fitting the remaining five parameters.

A linear least squares fit was performed using 46 lines to obtain spectroscopic constants (Table 5). Best fit to the experimental values was attained with a rotational temperature of 75 K and linewidth of 0.16 cm^{-1}. The spectral parameters estimated from the simulations for $^{11}B_3$ are B'': $C'' = 1.2246(45)$: $0.62131(72)$ cm^{-1} for the $\tilde{X}\,^2A_1'$ ground state and B': $C' = 1.1914(44)$: $0.61173(69)$ cm^{-1} for the $2\,^2E'$ excited state (Table 6). There is a modest difference between the inferred rotational constants from the fit and the calculated ones (Table 2). This implies that there is indeed a slight geometrical distortion during excitation from the ground state due to a Jahn-Teller effect in the $^2E'$ state as predicted theoretically [9] but neglected in this model for simplicity.

The rotational constants in this study are nearly two percent greater than those measured earlier using cavity ringdown absorption (four percent in the case of C) [6]. This is due to a number of reasons, including the fact that the previous analysis risked including lines not necessarily related to $^{11}B_3$, therefore affecting the result. In this study, where only $^{11}B_3$ lines are unambiguously identified, a better agreement with theory is obtained. Coriolis coupling has also been introduced as a parameter in addition to T_0, B'', B', A'', and A'. The previously recorded CRDS spectrum, on the other hand, was fitted while neglecting ζ because of line congestion, which has a direct influence on the values of the excited state constants. Also of note is the fact that the CRDS absorption study was hindered by the presence of large and broadened neon atomic lines, thus obscuring the true shape of the molecular band. Through mass selective

means we have been able to reassign the location of the origin, T_0, at 21848.77(2) cm^{-1} (previously 21853.52 cm^{-1} [6]).

4. Conclusion

The rotationally resolved excitation spectrum of the origin band for the $^2E' - \tilde{X}\,^2A_1'$ transition of cyclic-B (D_{3h}) has been recorded and analyzed. The mass selective technique of R2C2PI allowed the observation of the target species without the spectral congestion previously observed using CRDS, thus permitting the determination of a revised set of spectral constants to replace those derived previously [6]. Slight discrepancies with theoretically predictions indicate that Jahn-Teller effects in the excited state may complicate the spectrum and assignment.

References

[1] H. Ding, C. Apetrei, L. Chacaga, J.P. Maier, Astrophys. J. 627 (2008) 348.
[2] C. Apetrei, H. Ding, J.P. Maier, Phys. Chem. Chem. Phys. 9 (2007) 3897.
[3] E. Chasovskikh, E.B. Jochnowitz, E. Kim, J.P. Maier, I. Navizet, J. Phys. Chem. A 111 (2007) 11986.
[4] H. Ding, M.D. Morse, C. Apetrei, L. Chacaga, J.P. Maier, J. Chem. Phys. 125 (2006) 194315.
[5] H. Ding, M.D. Morse, J.P. Maier, Mol. Phys. 105 (2007) 1251.
[6] P. Cias, M. Araki, A. Denisov, J.P. Maier, J. Chem. Phys. 121 (2004) 6776.
[7] G. Herzberg, J. Chem. Phys. 70 (1979) 4806.
[8] I. Dabrowski, G. Herzberg, Can. J. Phys. 58 (1980) 1238.
[9] G. Herzberg, J.K.G. Watson, Can. J. Phys. 58 (1980) 1250.
[10] G. Herzberg, H. Lew, J.J. Sloan, J.K.G. Watson, Can. J. Phys. 59 (1981) 428.
[11] M. Vervloet, K.G. Watson, J. Mol. Spectrosc. 217 (2003) 255.
[12] H. Figger, H. Moller, W. Schrepp, H. Walther, Chem. Phys. Lett. 90 (1982) 90.
[13] H.-P. Helm, Phys. Rev. Lett. 56 (1986) 42.
[14] H.-P. Helm, Phys. Rev. A 38 (1988) 3425.
[15] A. Dodhy, W. Ketterle, H.-P. Messmer, H. Walther, Chem. Phys. Lett. 151 (1988) 133.
[16] I. Mistrík, R. Reichle, H.-P. Helm, U. Müller, Phys. Rev. A 63 (2001) 042711.
[17] M. Keil, H.-G. Kraemer, A. Kudell, M.A. Baig, J. Zhu, W. Demtroeder, W. Meyer, J. Chem. Phys. 113 (2000) 7414.
[18] H.A. Eckel, J.M. Gress, J. Biele, W. Demtroeder, J. Chem. Phys. 98 (1993) 135.
[19] Z. Fu, G.W. Lemire, Y.M. Hamrick, S. Taylor, J.-C. Shui, M.D. Morse, J. Chem. Phys. 88 (1988) 3524.
[20] A. OKe_e, J.J. Scherer, A.L. Cooksy, R. Sheeks, J. Heath, R.J. Saykally, Chem. Phys. Lett. 172 (1990) 214.
[21] I. Sioutis, V.L. Starkhursky, R.M. Pitzer, T.A. Miller, J. Chem. Phys. 126 (2007) 124309.
[22] S. Li, R.J. VanZee, W. Weltner, Chem. Phys. Lett. 262 (1996) 298.
[23] R.J.V.Y.M. Hamrick, W. Weltner, J. Chem. Phys. 96 (1992) 1767.
[24] A. Batalov, J. Fulara, I. Shnitko, J.P. Maier, Chem. Phys. Lett. 404 (2005) 315.
[25] M. Wyss, E. Riaplov, A. Batalov, J.P. Maier, T. Weber, W. Meyer, P. Rosmus, J. Chem. Phys. 119 (2003) 9703.
[26] J.M.L. Martin, J.P. Francois, R. Gijbels, J. Chem. Phys. 90 (1989) 6469.
[27] R. Hernandez, J. Simons, J. Chem. Phys. 94 (1991) 2961.
[28] A.D. Becke, J. Chem. Phys. 98 (1993) 5648.
[29] D.E. Woon, T.H. Dunning, J. Chem. Phys. 98 (1993) 1358.

[30] (a) J. Werner, P.J. Knowles, J. Chem. Phys. 82 (1985) 5053;
(b) J. Werner, P.J. Knowles, J. Chem. Phys. 89 (1988) 5803.
[31] M. J. Frisch, G. W. Trucks, H. B. Schlegel, G. E. Scuseria, M. A. Robb, J. R. Cheese-man, V. G. Zakrzewski, J. A. Montgomery, Jr., R. E. Stratmann, J. C. Burant, S. Dapprich, J. M. Millam, A. D. Daniels, K. N. Kudin, M. C. Strain, O. Farkas, J. Tomasi, V. Barone, M. Cossi, R. Cammi, B. Mennucci, C. Pomelli, C. Adamo, S. Clifford, J. Ochterski, G. A. Petersson, P. Y. Ayala, Q. Cui, K. Morokuma, D. K. Mal-ick, A. D. Rabuck, K. Raghavachari, J. B. Foresman, J. Cioslowski, J. V. Ortiz, A. G. Baboul, B. B. Stefanov, G. Liu, A. Liashenko, P. Piskorz, I. Komaromi, R. Gomperts, R. L. Martin, D. J. Fox, T. Keith, M. A. Al-Laham, C. Y. Peng, A. Nanayakkara, C. Gonzalez, M. Challacombe, P. M. W. Gill, B. G. Johnson, W. Chen, M. W. Wong, J. L. Andres, M. Head-Gordon, E. S. Replogle, J. A. Pople, GAUSSIAN 98 (Revision A.7), Gaussian, Inc., Pittsburgh, PA, 1998.
[32] H.-J. Werner, P. J. Knowles, R. Lindh, F. R. Manby, M. Schütz, P. Celani, T. Korona, G. Rauhut, R. D. Amos, A. Bernhardsson, A. Berning, D. L. Cooper, M. J. O. Deegan, A. J. Dobbyn, F. Eckert, C. Hampel, G. Hetzer, A. W. Lloyd, S. J. McNicholas, W. Meyer, M. E. Mura, A. Nicklaß, P. Palmieri, R. Pitzer, U. Schumann, H. Stoll, A. J. Stone, R. Tarroni, T. Thorsteinsson, Molpro, Version 2002.6, a 295 package of ab initio programs.
[33] C.M. Western, PGOPHER, A Program for Simulating Rotational Structure, University of Bristol, http://pgopher.chm.bris.ac.uk, 2007.
[34] G. Herzberg, Electronic Spectra and Electronic Structure of Polyatomic Molecules, Vol. III of Molecular Spectra and Molecular Structure, National Research Council of Canada, 1967.
[35] C.H. Townes, A.L. Schawlow, Microwave Spectroscopy, Dover Publications Inc., New York, 1975.